AAS 18-357

ANALYSIS AND DESIGN OF COLLISION AVOIDANCE MANEUVERS FOR PASSIVE DE-ORBITING MISSIONS

Juan Luis Gonzalo*, Camilla Colombo†, and Pierluigi Di Lizia‡

Collision avoidance maneuvers (CAMs) for passive de-orbiting missions using sails are studied, maneuvering either the sail or the incoming object. Analytical expressions for the CAM are obtained leveraging the proximal motion equations, maximizing the total or b-plane-contained deviation, or minimizing collision probability. When the sail performs the CAM, different attitude-related strategies are investigated. Representative test cases are proposed using data from ESA's MASTER tool or conjunction data messages. The required amount of propellant or sail maneuverability as function of lead time is traded-off, and the evolution in time of the covariance matrix is investigated.

INTRODUCTION

The ever-increasing proliferation of objects in Earth orbit, both operational satellites and space debris, poses a critical threat to the safe and sustainable use of space. Interest on this topic has been additionally furthered by recent developments in the space sector, such as new launch companies driving down the access cost to space, the popularization of small, cube and nanosats as affordable yet flexible platforms, and the large constellations being proposed both by incumbent companies and start-ups. Several international efforts are being undertaken to tackle this key issue, such as the Inter-Agency Space Debris Coordination Committee (IADC) and its space debris mitigation guidelines: a maximum lifetime of 25 years for objects in Low Earth Orbit (LEO), and the relocation to graveyard orbits for objects in Geostationary Earth Orbit (GEO).

However, complying with these, or similar, guidelines introduces additional costs and complexity. For instance, if a mitigation maneuver is to be performed using the satellite thrusters the additional operational time and propellant requirements have to be considered. Furthermore, this may not be a feasible option for all kinds of platforms. A cost-effective alternative for reducing the de-orbiting time of small satellites can be the use of passive end-of-life de-orbiting methods, such as drag or solar sails and electrodynamic tethers. For objects already in orbit, these solutions could also be applied through so called de-orbiting kits deployed by a servicing spacecraft. On the downside, their relatively large cross-sectional area appreciably increases the risk of collision with other spacecraft or space debris. The net effect of using these passive de-orbiting methods on the space environment around Earth is currently being evaluated by the European Space Agency-funded study "Environmental aspects of passive de-orbiting devices."[1,2]

This work deals with the design of collision avoidance maneuvers (CAMs) for end-of-life de-orbiting missions using drag or solar sails, considering the possibility of maneuvering either the de-orbiting satellite or the incoming object. By leveraging proximal motion equations, analytical expressions are obtained for the optimal direction of the deviating actions in the impulsive case.[3–5] Different solutions are obtained and compared by seeking to maximize either the total deviation or the deviation inside the b-plane of the nominal conjunction, or to minimize the collision probability. The validity of the proximal motion solutions for the intended application is assessed by comparing them with high-precision numerical propagations. A set of

*Postdoctoral research fellow, Department of Aerospace Science and Technology, Politecnico di Milano, Via la Masa 34, 20156 Milan, Italy
†Associate professor, Department of Aerospace Science and Technology, Politecnico di Milano, Via la Masa 34, 20156 Milan, Italy
‡Assistant professor, Department of Aerospace Science and Technology, Politecnico di Milano, Via la Masa 34, 20156 Milan, Italy

representative test cases is proposed by selecting several currently active satellites and using ESA's Meteoroid and Space Debris Terrestrial Environment Reference (MASTER) tool[6] to estimate the relative velocity of a possible conjunction at any given point of the satellite's orbit. Special attention is paid to assess the qualitative and quantitative effects of orbit eccentricity, conjunction geometry, and lead time to conjunction in the optimal direction of the deviating actions and the attainable deviation. Furthermore, the evolution of the covariance matrix with the time to impact is also considered, to check whether the growth of the uncertainties introduces a practical limit to the lead time for the CAM.[7] On the other hand, for the case in which the sail is the one to perform the CAM a simple yet effective control strategy is proposed. The effectiveness of this strategy is investigated by considering a test case taken from an actual conjunction data message, and several area-to-mass ratios (which is identified as the 'control authority' for the sail). Finally, the required amount of propellant or the sail area-to-mass ratio as function of the lead time to conjunction is evaluated and traded off for the different CAM strategies.

THEORETICAL APPROACH

Given a close approach (CA) between an active satellite and a debris, the objective is to perform a CAM to maximize the miss distance (or minimize the collision probability). For a satellite avoiding a debris or a de-orbiting sail, the CAM is assumed to be an impulsive maneuver performed at a certain time t_{CAM} before the time of CA t_{CA}. The lead time for the maneuver is then $\Delta t = t_{\mathrm{CA}} - t_{\mathrm{CAM}}$, and the instantaneous change in velocity due to the maneuver is called $\delta\mathbf{v}$. This impulsive maneuver can be modeled through Gauss planetary equations,[3,8] giving a relation between $\delta\mathbf{v}$ and the instantaneous change in the Keplerian elements in the form:

$$\delta\boldsymbol{\alpha}(t_{\mathrm{CAM}}) = \mathbf{G}_v(t_{\mathrm{CAM}})\,\delta\mathbf{v}(t_{\mathrm{CAM}})\,, \tag{1}$$

where $\delta\boldsymbol{\alpha} = [\,\delta a\ \delta e\ \delta i\ \delta\Omega\ \delta\omega\ \delta M\,]^{\mathrm{T}}$ are the changes in semi-mayor axis, eccentricity, inclination, right ascension of the ascending node, argument of perigee, and mean anomaly, respectively, and $\mathbf{G}_v(t_{\mathrm{CAM}})$ is the matrix form of the Gauss planetary equations at the time where the CAM is performed.[3] The deviation of the spacecraft at t_{CA} can now be computed analytically from $\delta\boldsymbol{\alpha}$ using relative motion equations.[3,9] In matrix form:

$$\delta\mathbf{r}(t_{\mathrm{CA}}) = \mathbf{A}_r(t_{\mathrm{CA}})\,\delta\boldsymbol{\alpha}(t_{\mathrm{CAM}})\,, \tag{2}$$

where $\mathbf{A}_r(t_{\mathrm{CA}})$ is the matrix form of the linearized relative motion equations. By combining the previous equations, a State Transition Matrix (STM) mapping changes in velocity at t_{CAM} with changes in position at t_{CA} is reached:

$$\delta\mathbf{r}(t_{\mathrm{CA}}) = \mathbf{A}_r(t_{\mathrm{CA}})\,\mathbf{G}_v(t_{\mathrm{CAM}})\,\delta\mathbf{v}(t_{\mathrm{CAM}}) = \mathbf{T}\,\delta\mathbf{v}(t_{\mathrm{CAM}})\,. \tag{3}$$

Although this expression is enough for the analytic modeling of CAMs, it would also be convenient to have the full STM mapping changes in the state at t_{CAM} with changes in the state at t_{CA}. Particularly, this would allow to propagate covariance matrices analytically instead of requiring computationally expensive methods like Monte-Carlo simulations. The change in Keplerian elements due to a change in state at t_{CAM} can be written as:

$$\delta\boldsymbol{\alpha}(t_{\mathrm{CAM}}) = \begin{bmatrix}\ \mathbf{G}_r(t_{\mathrm{CAM}}) & \mathbf{G}_v(t_{\mathrm{CAM}})\ \end{bmatrix}\delta\mathbf{s}(t_{\mathrm{CAM}}) = \mathbf{G}(t_{\mathrm{CAM}})\,\delta\mathbf{s}(t_{\mathrm{CAM}})\,, \tag{4}$$

where $\delta\mathbf{s} = [\,\delta\mathbf{r}\ \delta\mathbf{v}\,]^{\mathrm{T}}$. Same as before, the change in state at t_{CA} is obtained using relative motion equations:

$$\delta\mathbf{s}(t_{\mathrm{CA}}) = \begin{bmatrix}\ \mathbf{A}_r(t_{\mathrm{CA}})\ \\ \ \mathbf{A}_v(t_{\mathrm{CA}})\ \end{bmatrix}\delta\boldsymbol{\alpha}(t_{\mathrm{CAM}}) = \mathbf{A}(t_{\mathrm{CA}})\,\delta\boldsymbol{\alpha}(t_{\mathrm{CAM}})\,. \tag{5}$$

Combining both equations:

$$\delta\mathbf{s}(t_{\mathrm{CA}}) = \mathbf{A}(t_{\mathrm{CA}})\,\mathbf{G}(t_{\mathrm{CAM}})\,\delta\mathbf{s}(t_{\mathrm{CAM}}) = \overline{\mathbf{T}}\,\delta\mathbf{s}(t_{\mathrm{CAM}})\,. \tag{6}$$

It is straightforward to check that $\overline{\mathbf{T}}$ is a square matrix of dimension 6×6, and that the reduced STM $\mathbf{T}$ corresponds to the 3×3 upper-right block of $\overline{\mathbf{T}}$.

It is important to note that the expressions for $\mathbf{T}$, $\overline{\mathbf{T}}$, $\mathbf{A}$ and $\mathbf{G}$ will depend on the reference frames used to project $\delta\mathbf{s}(t_{\text{CAM}})$ and $\delta\mathbf{s}(t_{\text{CA}})$. Let us consider two different reference frames: a TNH frame at t_{CAM} and a RTH frame at t_{CA}. The TNH frame $\mathcal{T} = \{S; t, n, h\}$ is centered at the spacecraft's position at the CAM, and its axis are given by the tangential direction (i.e. along the velocity), the normal direction (inward belonging to the orbital plane), and the perpendicular-to-the-orbit-plane direction. The RTH frame $\mathcal{R} = \{S; r, \theta, h\}$ is also centered at the spacecraft, and its axis are oriented along the radial, transversal, and perpendicular-to-the-orbit-plane directions, respectively.

The expression for $\mathbf{G}_v$ with $\delta\mathbf{v}$ in TNH can be found in the literature:[3,8]

$$\mathbf{G}_v(t_{\text{CAM}}) = \begin{bmatrix} \frac{2a^2 v}{\mu} & 0 & 0 \\ \frac{2(e+\cos\theta)}{v} & -\frac{r}{av}\sin\theta & 0 \\ 0 & 0 & \frac{r\cos\theta^*}{h} \\ 0 & 0 & \frac{r\sin\theta^*}{h\sin i} \\ \frac{2\sin\theta}{ev} & \frac{2e+(r/a)\cos\theta}{ev} & -\frac{r\sin\theta^*\cos i}{h\sin i} \\ -\frac{b}{eav}2\left(1+\frac{e^2 r}{p}\right)\sin\theta & -\frac{b}{eav}\frac{r}{a}\cos\theta & 0 \end{bmatrix}, \tag{7}$$

where μ is the gravitational constant of the Earth, θ is the true anomaly, $\theta^* = \theta + \omega$ is the argument of latitude, b is the semi-minor axis of the nominal orbit, p is its parameter, and h is the norm of the angular momentum. On the other hand, the expression for $\mathbf{G}_r$ had to be developed for this study, following the same procedure outlined for $\mathbf{G}_v$ in the book by Battin:[8]

$$\mathbf{G}_r(t_{\text{CAM}}) = \begin{bmatrix} \frac{2a^2}{r^3}r_t & \frac{2a^2}{r^3}r_n & 0 \\ \frac{1}{\mu ae}\left(\frac{h^2 a}{r^3}-v^2\right)r_t + \frac{r\sin\theta}{ah}v & \frac{1}{\mu ae}\left(\frac{h^2 a}{r^3}-v^2\right)r_n & 0 \\ 0 & 0 & \frac{\sin\theta^*+e\sin\omega}{p} \\ 0 & 0 & -\frac{\cos\theta^*+e\cos\omega}{p\sin i} \\ G_{51}r_t + G_{52}v & G_{51}r_n & G_{53} \\ G_{61}r_t + G_{62}v & G_{61}r_n & 0 \end{bmatrix}, \tag{8}$$

with

$$G_{51} = -\frac{r}{h^2 e}\sin\theta\left(\frac{h^2}{pr^3}\left(p+e^2 r\right) - \frac{(p+r)v^2}{r^2}\right), \quad G_{52} = -\frac{r}{hep}\left(\cos\theta + e\right),$$
$$G_{53} = \left(\cos\theta^* + e\cos\omega\right)\frac{\cos i}{p\sin i}, \quad G_{61} = \frac{rb}{ha^2 e}\frac{h}{pr^3}\left(r^2 - a(p+r)\right)\sin\theta, \quad G_{62} = \frac{rb}{ha^2 e}\cos\theta,$$

where r_t and r_n are the tangential and normal components of $\mathbf{r}(t_{\text{CAM}})$, respectively.

Similarly, the expression for $\mathbf{A}_r$ with $\delta\mathbf{r}$ in RTH can be obtained from Schaub and Junkins,[9] taking into account that δM at t_{CA} includes the effects of both its variation at t_{CAM} and the change in mean motion:[3]

$$\mathbf{A}_r^{\text{T}}(t_{\text{CA}}) = \begin{bmatrix} \frac{r}{a} - \frac{3}{2}\frac{e\sin\theta}{\eta}\frac{\sqrt{\mu}}{a^{3/2}}\Delta t & -\frac{3}{2}\frac{r}{\eta^3}\left(1+e\cos\theta\right)^2\frac{\sqrt{\mu}}{a^{5/2}}\Delta t & 0 \\ -a\cos\theta & \frac{r\sin\theta}{\eta^2}\left(2+e\cos\theta\right) & 0 \\ 0 & 0 & r\sin\theta^* \\ 0 & r\cos i & -r\cos\theta^*\sin i \\ 0 & r & 0 \\ \frac{ae\sin\theta}{\eta} & \frac{r}{\eta^3}\left(1+e\cos\theta\right)^2 & 0 \end{bmatrix}, \tag{9}$$

where $\eta = \sqrt{1-e^2}$. Finally, the linearized expressions for the change in relative velocity are not explicitly

given in Schaub and Junkins,[9] but they are straightforward to develop:

$$\mathbf{A}_v^{\mathrm{T}}(t_{\mathrm{CA}}) = \begin{bmatrix} -\frac{eh\sin\theta}{2ap} - \frac{3}{2}\frac{ah(p-r)}{\eta r^3}\frac{\sqrt{\mu}}{a^{5/2}}\Delta t & -\frac{3}{2}\frac{h}{ar} + \frac{3}{2}\frac{aeh\sin\theta}{\eta r^2}\frac{\sqrt{\mu}}{a^{5/2}}\Delta t & 0 \\ \frac{ah\sin\theta}{r^2} & \frac{h}{p\eta^2}\left(e+\cos\theta\right) + \frac{ah}{r^2}\cos\theta & 0 \\ 0 & 0 & \frac{h}{p}\left(e\cos\omega + \cos\theta^*\right) \\ 0 & \frac{eh}{p}\cos i\sin\theta & \frac{h\sin i}{p}\left(e\sin\omega + \sin\theta^*\right) \\ 0 & \frac{eh}{p}\sin\theta & 0 \\ \frac{ah}{\eta r^3}(p-r) & -\frac{aeh}{\eta r^2}\sin\theta & 0 \end{bmatrix}. \tag{10}$$

A more convenient representation of the spacecraft's deviation can be achieved using the plane orthogonal to the relative velocity of the spacecraft with respect to the debris at the nominal CA. This is known as the b-plane,[10] and can be defined through a local reference frame $\mathcal{B} = \{D; \xi, \eta, \zeta\}$ centered at the debris D, with the η axis normal to the b-plane (i.e. oriented along the spacecraft's relative velocity), the ζ axis along the direction opposite to the projection of the debris velocity onto the b-plane, and the ξ axis completing a positively oriented reference system. Calling $\mathbf{v}_D$ and $\mathbf{v}_{SC}$ to the velocities of debris and spacecraft, respectively, the unity vectors for this reference system take the form:

$$\hat{\eta} = \frac{\mathbf{v}_{SC} - \mathbf{v}_D}{||\mathbf{v}_{SC} - \mathbf{v}_D||}, \qquad \hat{\xi} = \frac{\mathbf{v}_D \times \hat{\eta}}{||\mathbf{v}_D \times \hat{\eta}||}, \qquad \hat{\zeta} = \hat{\xi} \times \hat{\eta}. \tag{11}$$

One of the main advantages of using the b-plane for the design of CAMs is that displacements in the ζ axis are associated with a phasing maneuver (i.e., time shift), whereas displacements in the ξ axis come from a geometrical change in the spacecraft's orbit to change the MOID. For this reason, from now ζ will be referred to as the time axis, and ξ will be called geometry axis. It is also useful to define the impact parameter b^* as the intersection of the incoming asymptote and the b-plane. Assuming that the hyperbolic trajectory of the spacecraft with respect to the debris is nearly rectilinear, b^* will be a good approximation of the minimum miss distance.[3] Furthermore, b^* will also be close to the actual intersection of the spacecraft's trajectory with the b-plane. Abusing notation, from now on the distance between the debris and the spacecraft on the b-plane will be referred to as impact parameter, although the symbol b will be used instead of b^* to prevent confusion.

The b-plane projection of $\delta\mathbf{r}$ can be expressed in matrix form as:[11]

$$\delta\mathbf{b} = \mathbf{M}_{\delta\mathbf{b}}\delta\mathbf{r}\,, \qquad \text{with} \quad \mathbf{M}_{\delta\mathbf{b}} = \begin{bmatrix} \hat{\eta}_2^2 + \hat{\eta}_3^2 & -\hat{\eta}_1\hat{\eta}_2 & -\hat{\eta}_1\hat{\eta}_3 \\ -\hat{\eta}_1\hat{\eta}_2 & \hat{\eta}_1^2 + \hat{\eta}_3^3 & -\hat{\eta}_2\hat{\eta}_3 \\ -\hat{\eta}_1\hat{\eta}_3 & -\hat{\eta}_2\hat{\eta}_3 & \hat{\eta}_1^2 + \hat{\eta}_2^2 \end{bmatrix}, \tag{12}$$

where $\hat{\eta}_1$, $\hat{\eta}_2$, and $\hat{\eta}_3$ are the components of unity vector $\hat{\eta}$, expressed in the same reference frame as $\delta\mathbf{r}$. Then, the deviation in the b-plane for a given $\delta\mathbf{v}$ is:

$$\delta\mathbf{b} = \mathbf{M}_{\delta\mathbf{b}}\mathbf{T}\,\delta\mathbf{v} = \mathbf{Z}\,\delta\mathbf{v}\,, \tag{13}$$

where $\mathbf{Z}$ is the corresponding STM.

Assuming a direct impact (zero miss distance at nominal CA), the objective function for the maximum deviation problem in terms of $\delta\mathbf{r}$ or $\delta\mathbf{b}$ can be written as:

$$J_{\delta r} = ||\delta\mathbf{r}|| = ||\mathbf{T}\,\delta\mathbf{v}|| = \delta\mathbf{v}^{\mathrm{T}}\,\mathbf{T}^{\mathrm{T}}\mathbf{T}\,\delta\mathbf{v}\,,$$
$$J_{\delta b} = ||\delta\mathbf{b}|| = ||\mathbf{Z}\,\delta\mathbf{v}|| = \delta\mathbf{v}^{\mathrm{T}}\,\mathbf{Z}^{\mathrm{T}}\mathbf{Z}\,\delta\mathbf{v}\,.$$

Following an approach proposed by Conway,[5] maximizing $J_{\delta r}$ is equivalent to maximizing the associated quadratic form $\mathbf{T}^{\mathrm{T}}\mathbf{T}$ by choosing a $\delta\mathbf{v}_{\mathrm{opt}}$ parallel to the eigenvector of $\mathbf{T}^{\mathrm{T}}\mathbf{T}$ conjugated to the maximum eigenvalue. It is important to note that the sign of $\delta\mathbf{v}_{\mathrm{opt}}$ is not defined as it does not affect the magnitude of the deviation.[3,5] Regarding the magnitude of the impulse, δv_{opt}, it is straightforward to check that the quadratic

form is maximized by using all the available impulse capability. The same procedure can be applied for the maximization of $J_{\delta b}$ by solving the eigenvalue problem for the associated quadratic form $\mathbf{Z}^{\mathrm{T}}\mathbf{Z}$.

Depending on the uncertainties in the positions of spacecraft and debris, the maximum deviation CAM may differ notably from the minimum collision probability one. In a recent work, Bombardelli and Hernando-Ayuso[12] proposed an approximate analytic method for designing minimum collision probability CAMs, using Chan's approach for the computation of collision probabilities[13,14] in order to reduce the optimization problem to a quadratic form similar to the one considered by Conway. First of all, the original conjunction in the b-plane, in which each object has its own spherical envelope and covariance matrix, is reduced to an equivalent problem by assigning a combined covariance to the debris (with no envelope) and a combined envelope to the spacecraft (with no covariance). The combined covariance:

$$\mathbf{C} = \begin{bmatrix} \sigma_\xi^2 & \rho_{\xi\zeta}\sigma_\xi\sigma_\zeta \\ \rho_{\xi\zeta}\sigma_\xi\sigma_\zeta & \sigma_\zeta^2 \end{bmatrix}, \tag{14}$$

can be calculated as the sum of the individual covariances for both objects, as long as their determination is statistically independent. Similarly, the radius r_A of the combined envelope is defined as the sum of the radii of the individual envelopes for each object. Then, following Chan's approach the collision probability between debris and spacecraft can be approximated through the convergent series:

$$P(u,v) = \mathrm{e}^{-v/2} \sum_{m=0}^{\infty} \frac{v^m}{2^m m!} \left(1 - \mathrm{e}^{-u/2} \sum_{k=0}^{m} \frac{u^k}{2^k k!} \right), \tag{15}$$

with

$$u = \frac{r_A^2}{\sigma_\xi \sigma_\zeta \sqrt{1-\rho_{\xi\zeta}^2}}, \qquad v = \left[\left(\frac{\xi}{\sigma_\xi} \right)^2 + \left(\frac{\zeta}{\sigma_\zeta} \right)^2 - 2\rho_{\xi\zeta} \frac{\xi}{\sigma_\xi} \frac{\zeta}{\sigma_\zeta} \right] / (1-\rho_{\xi\zeta}^2), \tag{16}$$

where (ξ, ζ) is the position of the spacecraft in the b-plane at the CA. As shown by Chan,[13,14] accurate results can be obtained for $m = 3$ for small values of u. Interestingly, the position of the spacecraft only influences collision probability P through the depth of intrusion v. Then, it is possible to prove that minimizing P is equivalent to maximizing:[12]

$$J_P = \left(\frac{\xi}{\sigma_\xi} \right)^2 + \left(\frac{\zeta}{\sigma_\zeta} \right)^2 - 2\rho_{\xi\zeta} \frac{\xi}{\sigma_\xi} \frac{\zeta}{\sigma_\zeta} = \delta\mathbf{r}^{\mathrm{T}} \mathbf{Q}^* \delta\mathbf{r} = \delta\mathbf{b}^{\mathrm{T}} \mathbf{Q}^* \delta\mathbf{b}, \tag{17}$$

where $\delta\mathbf{r}$ and $\delta\mathbf{b}$ are projected in the b-plane, and:

$$\mathbf{Q}^* = \begin{bmatrix} 1/\sigma_\xi^2 & 0 & -\rho_{\xi\zeta}/\sigma_\xi\sigma_\zeta \\ 0 & 0 & 0 \\ -\rho_{\xi\zeta}/\sigma_\xi\sigma_\zeta & 0 & 1/\sigma_\zeta^2 \end{bmatrix}. \tag{18}$$

By substituting the expressions for $\delta\mathbf{b}$ or $\delta\mathbf{r}$, Eqs. (3) and (13), the problem is reduced to the maximization of a quadratic form of $\delta\mathbf{v}$, which can be solved in the same fashion as the maximum deviation case. The main difference between this study and the work by Bombardelli and Hernando-Ayuso is the choice of dynamical model: while they developed a STM based on the Dromo orbital elements (for which time is a dependent variable), we apply the previously introduced STM based on Gauss planetary equations and linear relative motion. The proposed approach has the advantage of not requiring the solution of the time equation for every variation of the orbit of the spacecraft, reducing computational cost.

CAM DESIGN AND SENSITIVITY ANALYSIS

The design of CAMs in different practical scenarios is now studied in detail, including extensive sensitivity analysis. Realistic test data is generated from current missions and ESA's MASTER 2009 tool. Maximum miss distance CAMs for a CA between a spacecraft and a debris are considered first, exploring the advantages

Table 1. Nominal orbital parameters for PROBA-2

ID	Epoch [UTC]	a [km]	e [-]	i [deg]	Ω [deg]	ω [deg]	M [deg]
36037	2018/04/20 03:18:34	7093.637	0.0014624	98.2443	303.5949	109.4990	250.7787

Table 2. Nominal orbital parameters for XMM

ID	Epoch [UTC]	a [km]	e [-]	i [deg]	Ω [deg]	ω [deg]	M [deg]
25989	2018/04/27 18:31:05	66926.137	0.8031489	70.1138	348.8689	95.9905	359.6770

of working in the b-plane. Then, the effect of uncertainties is included, comparing maximum deviation and minimum collision probability strategies, and assessing the effect of drag and Solar Radiation Pressure (SRP) in the evolution of the covariance matrix of a sail. Finally, a practical strategy for CAMs by a de-orbiting sail is proposed and studied.

Spacecraft against debris

The design of maximum miss distance CAMs for a spacecraft-debris CA is considered first. Although this configuration does not yet include a sail, it will serve to analyze the differences between maximizing total miss distance or impact parameter in the b-plane, as well as to perform a sensitivity analysis on the geometry of the CA.

Two test cases are selected from current ESA missions: a quasi-circular orbit (PROBA-2) and a highly elliptical orbit (XMM). Their nominal orbital parameters are summarized in Tables 1 and 2, respectively*. For the study, the nominal orbit geometry will be preserved (i.e semi-major axis, eccentricity, inclination, right ascension of the ascending node, and argument of perigee), whereas the position inside the orbit (i.e. the true anomaly) will be changed to study its influence in the CAM.

Regarding the debris, information from ESA's MASTER-2009[6] is used in order to cover a wide range of realistic conjunction geometries. For each position of the spacecraft in its nominal orbit, a set of possible debris orbits with zero miss distance at CA (direct impact) is constructed from the ranges in conjunction azimuth, elevation and relative velocity given by MASTER. In all cases, the sources for conjunctions are Launchers and Mission Related Objects (LMROs). The object flux distributions as functions of azimuth, elevation and relative velocity for PROBA-2 are shown in Fig. 1.

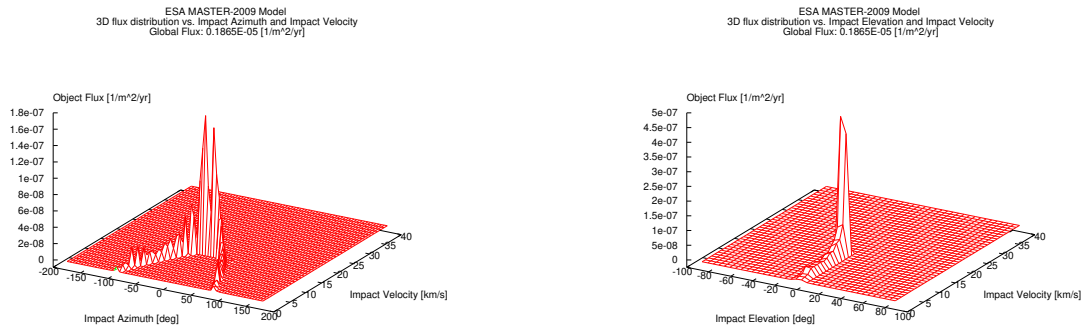

Figure 1. Debris object fluxes for PROBA-2 nominal orbit, as functions of azimuth, elevation and velocity at the conjunction.

*Orbit information retrieved from `http://www.heavens-above.com` [Last retrieved 30/04/2018]

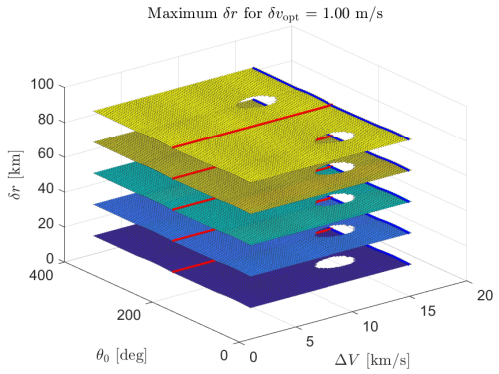

Figure 2. Maximum miss distance for PROBA-2 for an impulsive maneuver of 1 m/s. Each level corresponds to a different a lead time (from bottom to top, 1 to 5 periods of the spacecraft's orbit).

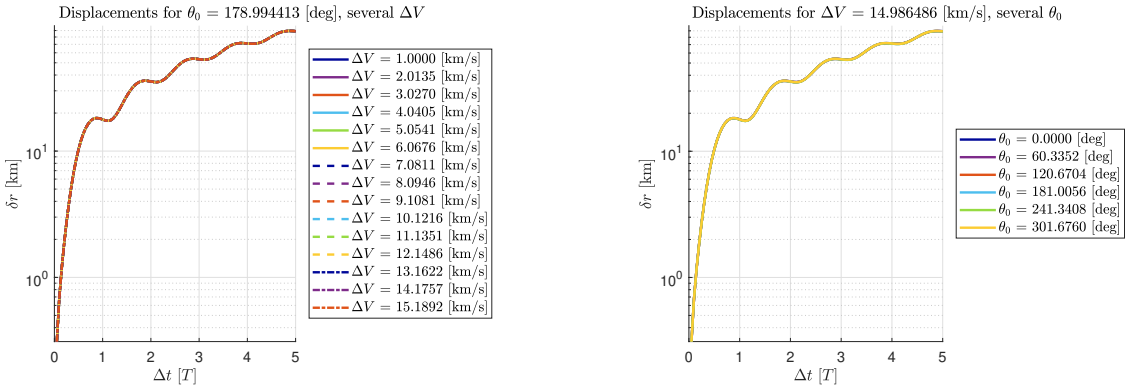

Figure 3. Maximum miss distance for PROBA-2 as a function of the maneuver lead time (impulsive maneuver magnitude of 1 m/s).

Since the magnitude of the impulsive maneuver does not affect its optimal direction in the linearized model, there are four free parameters to be considered in the sensitivity analysis: true anomaly of the spacecraft at the conjunction (θ_0), relative velocity between the spacecraft and the debris at the conjunction (ΔV), and azimuth and elevation angle (geometry at the conjunction). To present the data in a concise manner, the last two are removed by presenting only the case with the maximum miss distance (or impact parameter) for each combination of true anomaly and relative velocity.

The maximum δr results for PROBA-2 are presented in Figs. 2-3, for a δv_{opt} of 1 m/s. Since $\delta \mathbf{r}$ depends linearly with $\delta \mathbf{v}$ in the analytic model, results for a different δv_{opt} can be obtained by scaling. Figure 2 summarizes the effect of θ_0, ΔV and Δt in the attainable δr. The first two have a very small effect on the miss distance, whereas the lead time increases δr in a regular fashion. Note that no feasible conjunction was found for some combinations of θ_0 and ΔV, leading to holes in the isotime surfaces. Figure 3 represents the evolution of δr with lead time for fixed values of θ_0 and ΔV. For clarity, the corresponding fixed values have been also marked in Fig. 2, with a red line for θ_0 and a blue line for ΔV. As previously indicated, true anomaly and relative conjunction velocity have a negligible effect on the miss distance.

The effect of the eccentricity can be clearly appreciated in the results for the XMM test case, Figs. 4-5. While the variation of δr with ΔV is still negligible, it strongly depends on θ_0. Same as before, the fixed θ_0 and fixed ΔV plots in Fig. 5 correspond, respectively, to the red and blue lines in Fig. 4. Regarding the results for fixed ΔV and several θ_0, it is important to highlight how the best solution for each period corresponds

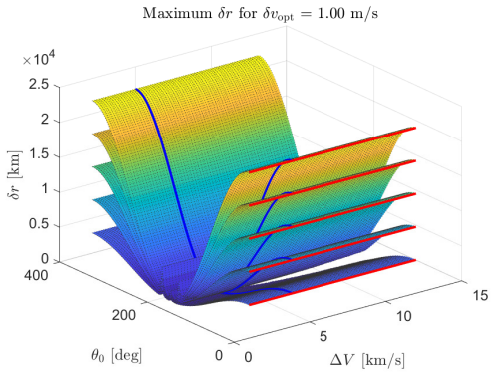

Figure 4. Maximum miss distance for XMM for an impulsive maneuver of 1 m/s. Each level corresponds to a different a lead time (from bottom to top, 1 to 5 periods of the spacecraft's orbit).

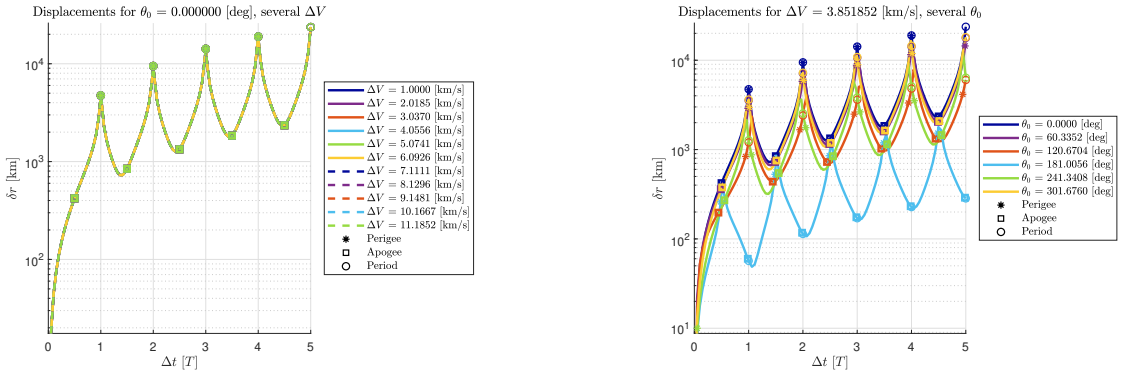

Figure 5. Maximum miss distance for XMM as a function of the maneuver lead time (impulsive maneuver magnitude of to 1 m/s).

to performing the maneuver close to the perigee, and that the highest δr is reached when the maneuver also coincides with a whole number of periods (i.e. when the CA takes place at the perigee). Conversely, minimum values for δr are obtained close to the apogees, and results worsen as the anomaly of the CA separates from the perigee of the maneuvering spacecraft's orbit.

We now present the results for the optimal maneuver maximizing the impact parameter in the b-plane, rather than the total miss distance. The maximum δb results show some key differences with respect to the maximum δr cases. As it can be seen in Figs. 6 and 9, the deflection in the b-plane is strongly influenced by the geometry of the conjunction. This is particularly important in the PROBA-2 (quasi-circular) test case, Figs. 6 and 7, where δb goes to zero as ΔV approaches 15 km/s. The reason for this lies in the evolution of the azimuth and elevation of the conjunction, Fig. 1, showing that the conjunction geometry becomes closer to a head-on collision as ΔV increases. For a head-on collision, trying to move along the time axis in the b-plane is ineffective, requiring a less efficient displacement in the geometry axis. The effect of ΔV in the elliptic case is much less important, Fig. 10, but slightly greater than for the maximum δr results. On the other hand, the phasing of the CA and the CAM with respect to the perigee of the spacecraft's orbit plays a very important role for the eccentric case, while the quasi-circular case now shows a small dependence with θ_0. Finally, the required δv_{opt} for a given δb of 5 km, Figs. 8 and 11, inherits the same qualitative behaviors already described for δb. Particularly, the CAM cost for the quasi-circular case rapidly increases as the relative velocity at conjunction approaches the maximum limit set from MASTER data.

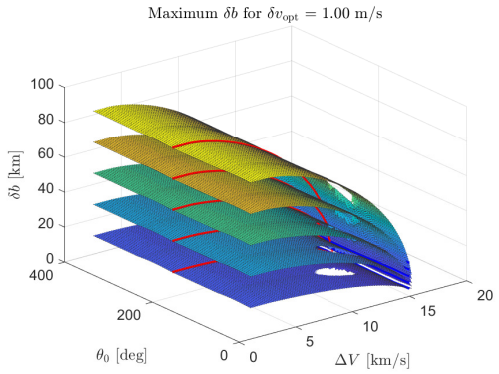

Figure 6. Maximum impact parameter for PROBA-2 for an impulsive maneuver of 1 m/s. Each level corresponds to a different a lead time (from bottom to top, 1 to 5 periods of the spacecraft's orbit).

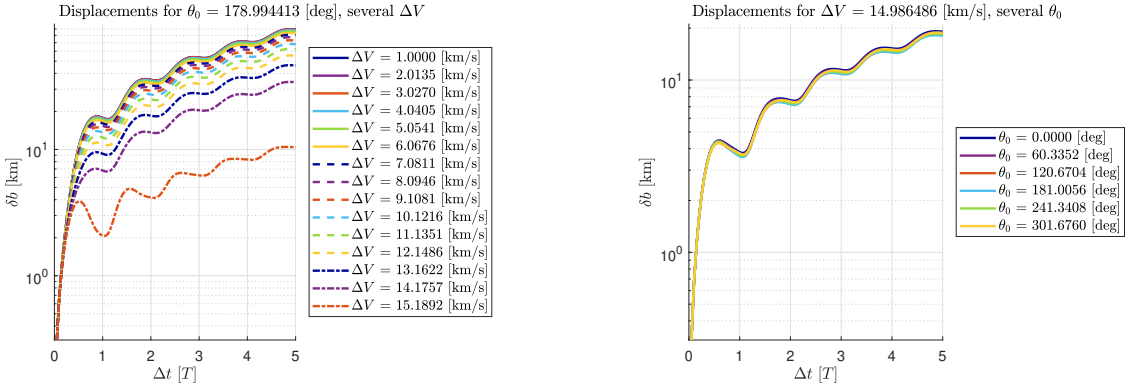

Figure 7. Maximum impact parameter for PROBA-2 as a function of the maneuver lead time (impulsive maneuver magnitude of 1 m/s).

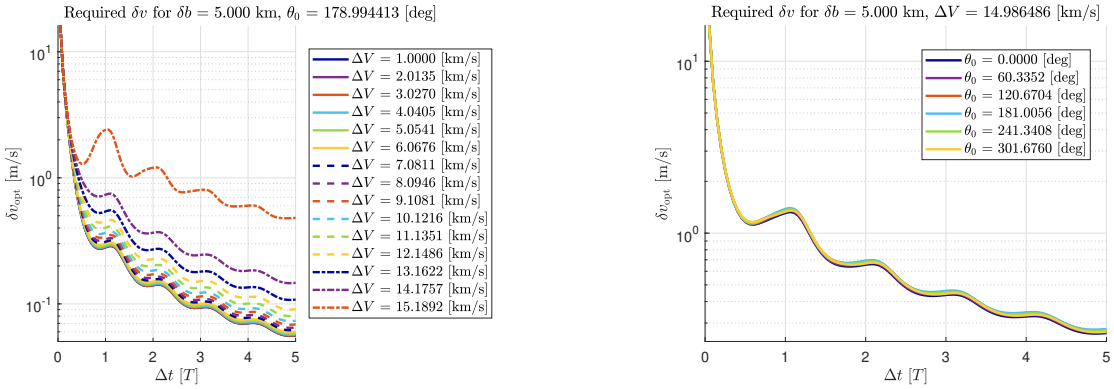

Figure 8. Required δv_{opt} to reach an impact parameter of 5 km for PROBA-2 as a function of the maneuver lead time.

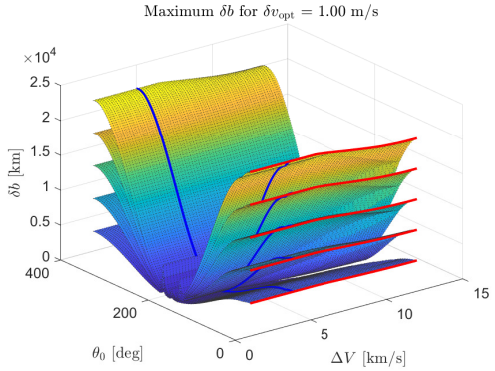

Figure 9. Maximum impact parameter for XMM for an impulsive maneuver of 1 m/s. Each level corresponds to a different a lead time (from bottom to top, 1 to 5 periods of the spacecraft's orbit).

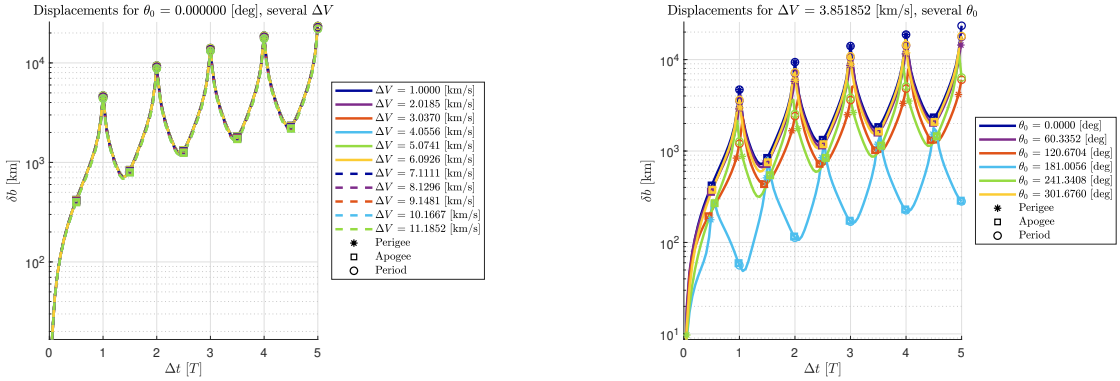

Figure 10. Maximum impact parameter for XMM as a function of the maneuver lead time (impulsive maneuver magnitude of 1 m/s).

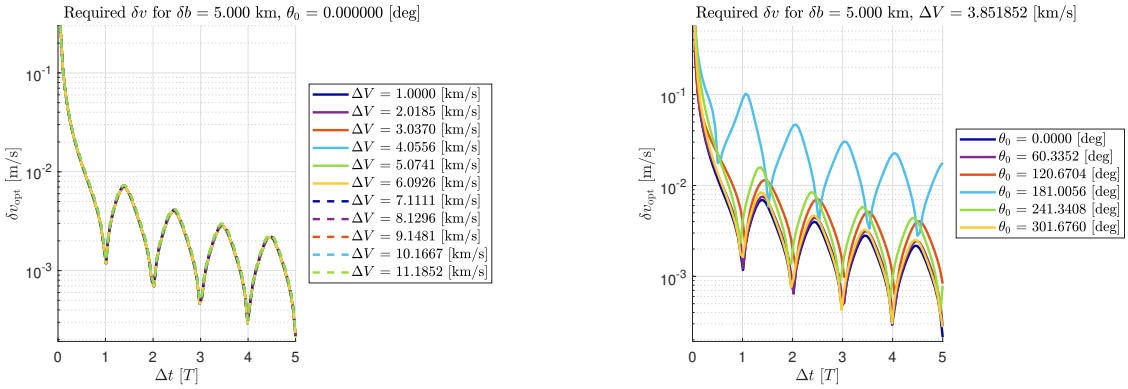

Figure 11. Required δv_{opt} to reach an impact parameter of 5 km for XMM as a function of the maneuver lead time.

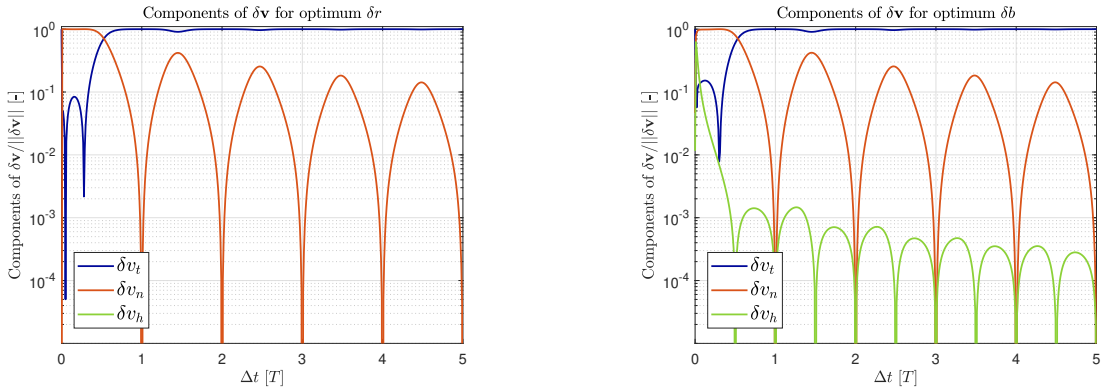

Figure 12. Optimal impulsive CAM components for the XMM test case, for the maximum miss distance (left) and maximum impact parameter (right) CAMs.

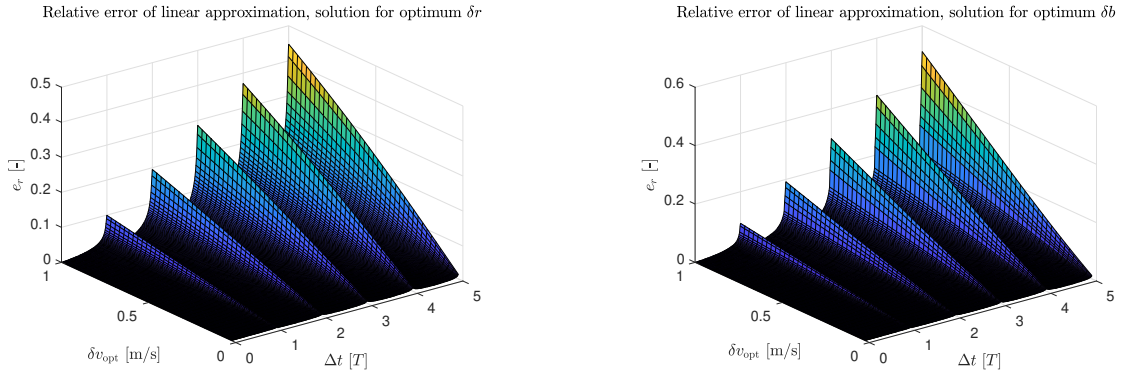

Figure 13. Relative errors for the deviation of XMM, for the maximum miss distance (left) and maximum impact parameter (right) CAMs.

The components of the optimum $\delta\mathbf{v}$ in TNH frame are represented in Fig. 12, for the XMM maximum δr and maximum δb CAMs. In both cases, the normal direction is dominant during the first half period, while the tangential direction becomes dominant for longer lead times. The out-of-plane component is generally negligible, but noticeably lager for the maximum δb maneuver.

To conclude this part of the study, the accuracy of the relative motion approximation is evaluated by comparing its predictions with a fully numeric propagation. A relative error is defined as:[3]

$$e_r = \frac{||\delta\mathbf{r}_{\text{propagated}} - \delta\mathbf{r}_{\text{estimated}}||}{||\delta\mathbf{r}_{\text{propagated}}||} \tag{19}$$

where $\delta\mathbf{r}_{\text{propagated}}$ is the deviation computed by the numerical propagation and $\delta\mathbf{r}_{\text{estimated}}$ is the deviation estimated by the analytic model. Figure 13 shows the relative errors for the XMM test case as a function of δv_{opt} and Δt, both for the maximum δr and maximum δb CAMs. In both cases the relative error grows with the maneuver lead time and δv_{opt}, because the accuracy of the relative motion approximation decreases as the separation between the nominal and modified orbits increases. The evolution with lead time shows a periodic behavior, with local maxima located at around whole periods.

Design of CAM with uncertainties. Spacecraft versus debris or sail

The previous section does not take into account the effect of uncertainties. Although the miss distance (or impact parameter) for a given impulse can be easily increased by considering a longer lead time, this will also

Table 3. Spacecraft and debris nominal Keplerian elements

	a [km]	e [-]	i [deg]	Ω [deg]	ω [deg]	θ_0 [deg]
PROBA-2	7093.637	0.0014624	98.2443	303.5949	109.4990	179.4986
Debris	7782.193	0.0871621	88.6896	142.7269	248.1679	1.2233

increase the uncertainties about the objects' position and velocity at the CA. This raises the question of what is the net effect of lead time on collision probability. Furthermore, the maximum miss distance (or impact parameter) CAM may not necessarily correspond to the minimum collision probability for a given δv_{opt}. For objects with large envelopes and uncertainties, designing the CAM to minimize the latter can prove to be more practical from an operational point of view.

To address this two key issues, maximum δb and minimum collision probability P CAMs are designed and compared for the spacecraft versus debris case.

The publicly available information about real covariance matrices and CAs is very limited, especially if sails are involved. For this test case, a sample covariance matrix numerically constructed from TLEs for an Iridium 33 debris (NORAD ID 33874) is used. The full covariance matrix (position and velocity) in ECI J2000 frame is:

$$\mathbf{C}|_{\text{ref}} = \begin{bmatrix} +1.1554\,10^{-02} & -2.3144\,10^{-03} & -1.1731\,10^{-03} & +4.5252\,10^{-07} & -5.6795\,10^{-07} & -1.0945\,10^{-05} \\ -2.3144\,10^{-03} & +1.9146\,10^{-02} & +1.4167\,10^{-02} & -1.2286\,10^{-05} & -2.5535\,10^{-06} & -3.3049\,10^{-06} \\ -1.1731\,10^{-03} & +1.4167\,10^{-02} & +3.0870\,10^{-01} & -2.8750\,10^{-04} & -8.6187\,10^{-05} & -1.2493\,10^{-06} \\ +4.5252\,10^{-07} & -1.2286\,10^{-05} & -2.8750\,10^{-04} & +2.8850\,10^{-07} & +7.9940\,10^{-08} & +1.1511\,10^{-09} \\ -5.6795\,10^{-07} & -2.5535\,10^{-06} & -8.6187\,10^{-05} & +7.9940\,10^{-08} & +4.5996\,10^{-08} & +1.4570\,10^{-09} \\ -1.0945\,10^{-05} & -3.3049\,10^{-06} & -1.2493\,10^{-06} & +1.1511\,10^{-09} & +1.4570\,10^{-09} & +1.2022\,10^{-08} \end{bmatrix}$$

with units of km and km/s for length and velocity, respectively. The position and velocity at orbit determination are:

$$\mathbf{r}_{\text{OD}} = \begin{bmatrix} +6.9687\,10^{+03} & +2.0930\,10^{+03} & -8.0909\,10^{+00} \end{bmatrix} \text{km}\,,$$
$$\mathbf{v}_{\text{OD}} = \begin{bmatrix} -1.5353\,10^{-01} & +4.4753\,10^{-01} & +7.3566\,10^{+00} \end{bmatrix} \text{km/s}\,.$$

The sample covariance matrix $\mathbf{C}|_{\text{ref}}$ is given at a particular orbital position. However, in order to perform the sensitivity analysis the covariance matrix at each maneuver time is needed. To address this issue, a procedure is devised to construct realistic covariance matrices for an arbitrary true anomaly. The aim is to preserve the size of the sample covariance ellipsoid, while updating its orientation. This is achieved by applying the eigenvalues of the original sample covariance matrix (representing its size) to the eigenvectors obtained after propagating the sample covariance up to desired true anomaly (representing the new orientation).

A sensitivity analysis is now performed for a CA taken from the previous PROBA-2 example. The nominal Keplerian elements of spacecraft and debris at CA are reported in Table 3, corresponding to a direct impact (zero distance at CA). Both objects are assigned a covariance matrix, constructed from $\mathbf{C}|_{\text{ref}}$ following the procedure previously introduced. Orbits and covariances are propagated using the analytic formulation.

The effect of lead time in the uncertainties is evaluated by assuming that orbit determination for each object is performed at maneuver time, and propagating the corresponding covariance matrix up to the CA. Figure 14 shows the evolution with Δt of the angle between the principal direction of the covariance ellipse in the b-plane and the time axis. The angle approaches 0 as the lead time increases, with periodic oscillations leading to local maxima around the perigee and local minima around the apogee after the first period.

The preference of the covariance ellipse to grow and align along the ζ axis is justified by the representation of dynamics in the b-plane, where the time axis ζ corresponds to the change in phasing and the geometry axis ξ to the orbit modification. Consequently, it is expected that the maximum δb CAM will also tend to align with the ζ axis as lead time increases. This behavior is verified in Fig. 15.

The fact that both uncertainties and miss distance grow along the same direction casts doubts about the efficiency of this approach to reduce collision probability. A better solution can be sought for by trying to

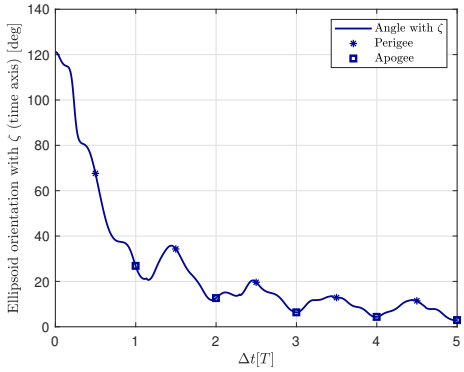

Figure 14. Orientation of the combined covariance ellipse in the b-plane with respect to ζ (time axis).

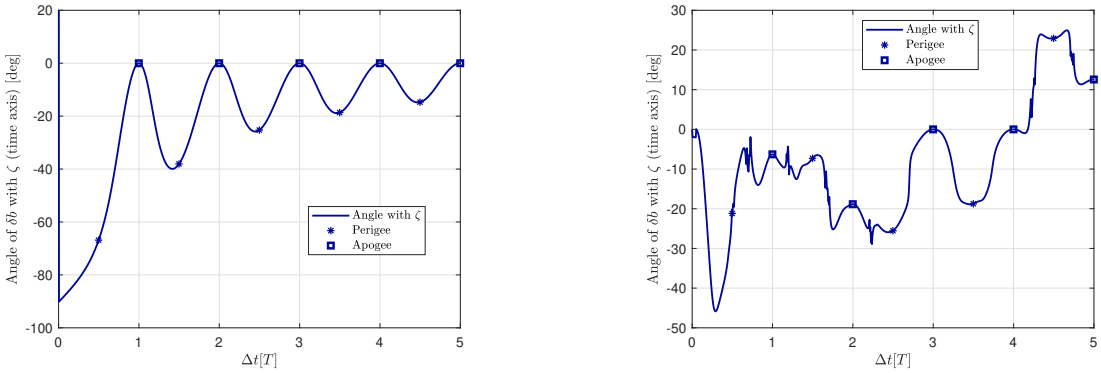

Figure 15. Orientation in the b-plane with respect to ζ (time axis) of the deviated position for the maximum δb (left) and minimum collision probability (right) solutions.

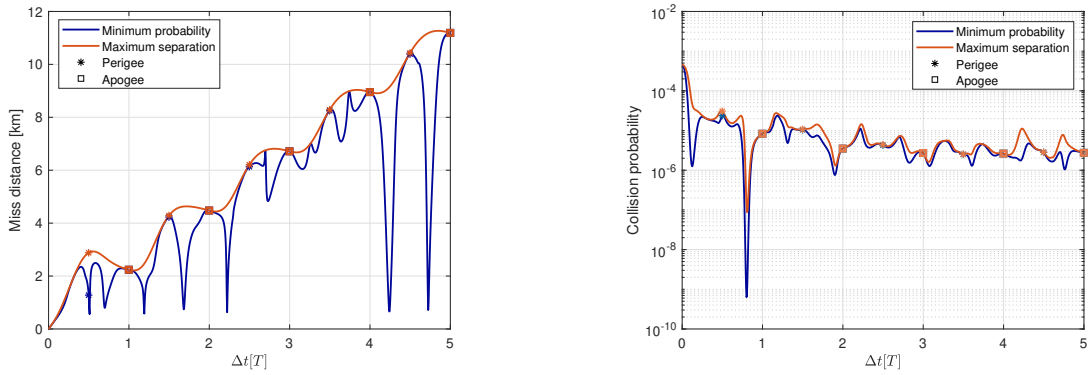

Figure 16. Miss distance in the b-plane (left) and collision probability (right) for the PROBA-2 test case, both for maximum impact parameter and minimum collision probability CAMs.

minimize collision probability directly. The minimum collision probability CAM is expected to not only try to increase the miss distance, but also to orient the deviation close to the semi-minor axis of the covariance ellipse. Figure 16 compares the results obtained for the maximum δb and minimum collision probability CAMs, both in terms of the miss distance in the b-plane and the collision probability. The differences between both solutions vary strongly with the lead time due to the evolution of the uncertainties, with some very notable features taking place for lead times within the first period. Furthermore, Fig. 15 confirms that the minimum collision probability solution tends to separate from the ζ axis more than the maximum δb solution.

The behavior of the two different strategies can be better understood by studying the evolution of the deviated trajectories in the b-plane. Figures 17-18 show the b-plane representations of the maximum impact parameter and minimum collision probability CAMs for two lead times smaller than one period. All cases have a δv_{opt} of 0.7 m/s, and a combined envelope radius r_A of $10\,\text{m}$. The first example, Fig. 17, corresponds to the first local minimum in collision probability from Fig. 16. As expected, the significant difference in collision probability between both CAM strategies is due to the relative orientations of the deviated trajectories with respect to the principal directions of the covariance ellipse, with the minimum collision probability CAM closely aligned with the smallest principal direction. Interestingly, the covariance ellipse and the maximum distance solutions are not yet aligned with the time axis, as the lead time is short.

The second example, Fig. 18, corresponds to the first local minimum of the miss distance for the minimum collision probability CAM. Same as before, the minimum collision probability solution aligns with the smallest principal direction of the covariance, although this comes at a large cost for the attainable miss distance. Conversely, the maximum impact parameter solution lies along the principal direction of the ellipse, achieving a notably higher miss distance but with an appreciably worse collision probability.

The evolution of the components of $\delta\mathbf{v}$ for each type of CAM are represented in Fig. 19. Both CAMs tend to align with the tangential direction for lead times greater than half a period of the spacecraft's orbit, but the minimum collision probability case presents small deviations and higher values of the other two components. Furthermore, the evolution with lead time of the uncertainties results in a less smooth short-term evolution of the control orientation.

If the debris is a sail, the perturbations from drag and SRP cannot be neglected. For the remainder of this subsection, the evolution of the covariance matrix under the effect of atmospheric drag and SRP is evaluated. The analytic STM is no longer valid, as it does not currently include these perturbations, so the covariance propagation for the debris is performed with Monte-Carlo methods. Orbit propagation is performed using averaged dynamics with PlanODyn.[15]

The evolution of the size and orientation of the combined covariance ellipse in the b-plane for the same test case in Table 3 is shown in Fig. 20. The drag and SRP coefficients are $c_D = 2.1$ and $c_R = 1.8$, respectively, and the area-to-mass ratio is $2\,\text{m}^2/\text{kg}$. The most notable conclusion is that for relatively short lead times, typical of practical collision avoidance scenarios, the effect of drag and SRP on the orientation and size of the combined covariance is small. Figure 21 shows the evolution of the covariances of the position in the b-plane reference frame. Same as before, the differences between the propagation with and without drag and SRP are small. The largest increase takes place along the direction normal to the b-plane, and the covariance along the geometry axis (σ_ξ) is bounded.

Since the CAM design for a spacecraft against a sail (with drag and SRP) presents the same qualitative characteristics already analyzed for a spacecraft against a debris (without drag and SRP), and the differences in covariance propagation are small for the lead times under consideration, the full analysis is not repeated here. To conclude this part of the study, the required δv_{opt} to achieve a collision probability of 10^{-5} for the previous test case and several radii of the combined envelope are shown in Fig. 22. As expected, the required δv_{opt} is smaller for the minimum collision probability case than for the maximum δb one, and it increases with the size of the envelope.

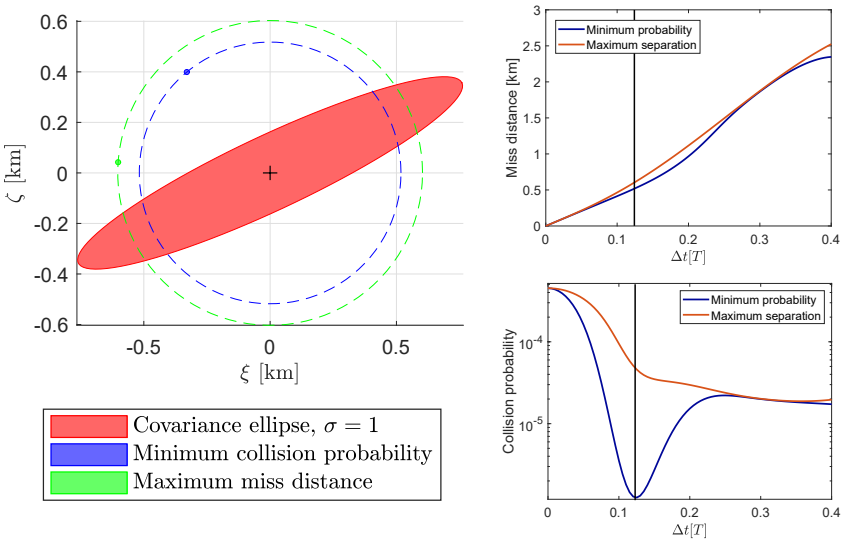

Figure 17. B-plane representation of different CAMs, for a lead time of 0.1241 periods of the spacecraft. Combined envelopes are plotted at scale, and circles in dashed lines represent the miss distance for each solution

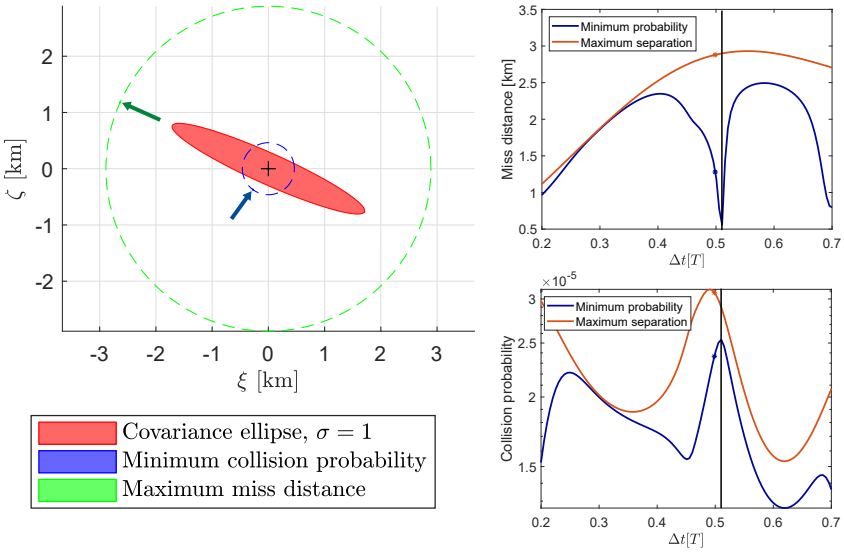

Figure 18. B-plane representation of different CAMs, for a lead time of 0.5095 periods of the spacecraft. Combined envelopes are plotted at scale, and circles in dashed lines represent the miss distance for each solution

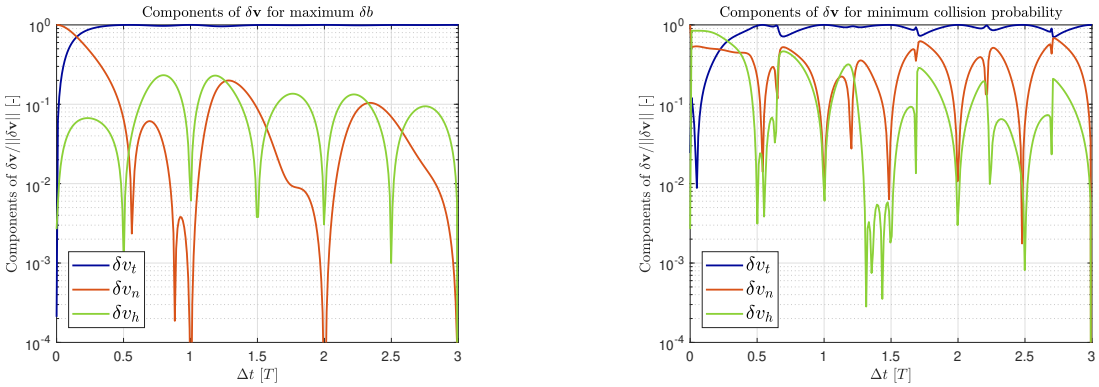

Figure 19. Optimal impulsive CAM components for the maximum δb (left) and minimum collision probability (right) strategies.

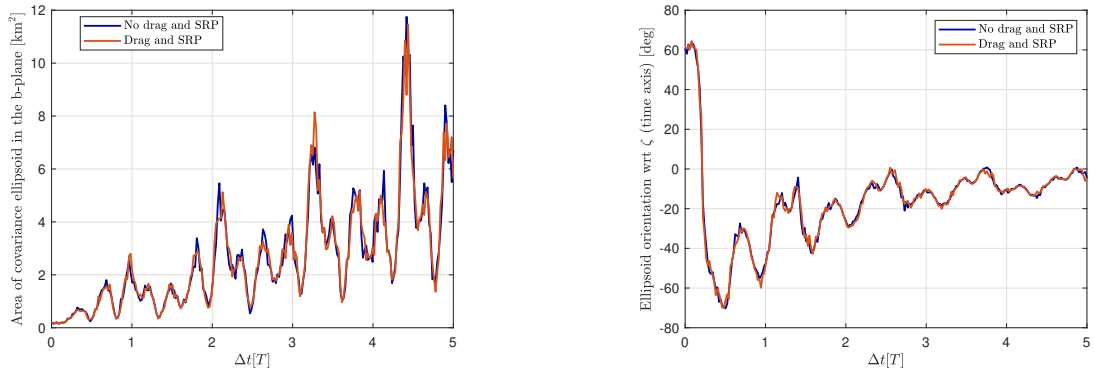

Figure 20. Comparison of the evolution of size and orientation of the combined covariance ellipse in the b-plane, with and without drag and SRP.

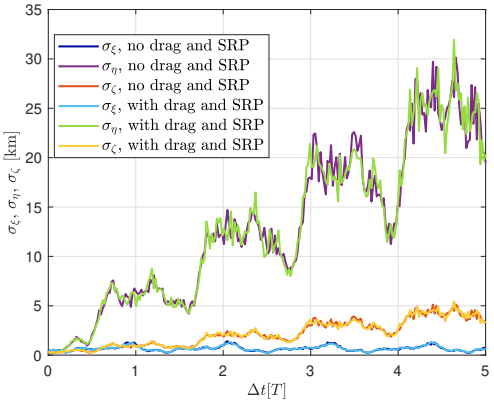

Figure 21. Evolution of the covariances of the position in the b-plane frame, with and without drag and SRP.

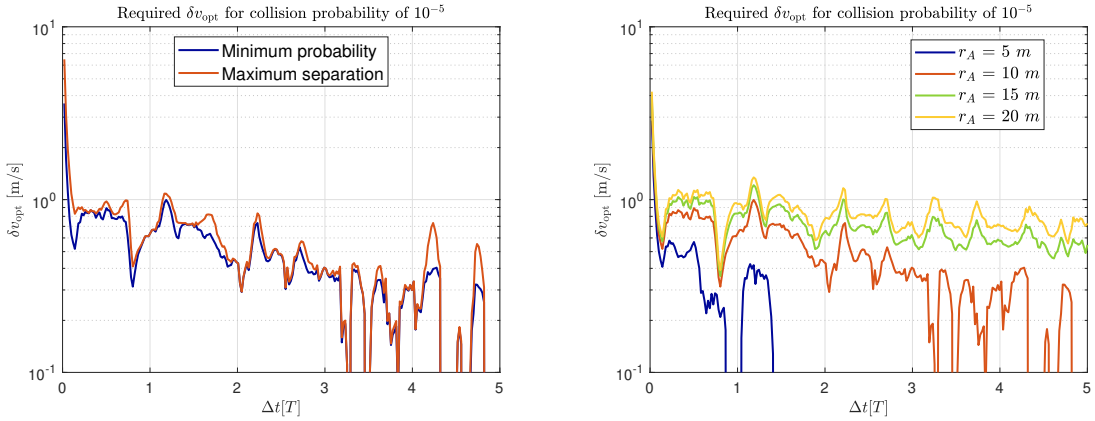

Figure 22. δv_{opt} required to achieve a collision probability of 10^{-5}. To the left, solutions for maximum δb and minimum collision probability CAMs with an evelope of 10 m. To the right, solutions for the minimum collision probability CAM and several envelope sizes.

Design and results for CAM by a de-orbiting sail

The last part of the study deals with the design of CAMs by a de-orbiting sail. From a conceptual point of view, one could consider two possibilities: 1) to change the sail orientation just before the CA in order to reduce the effective impact area in the b-plane; 2) to continuously control the orientation in time to reduce collision probability or increase miss distance. However, these strategies are severely limited by the control capabilities of the sail.[1,2] A simple yet effective control law can be devised by recalling the results for the spacecraft versus debris case, which showed that the impulsive $\delta\mathbf{v}$ tends to align with the tangential direction for lead times longer than half a period of the maneuvering spacecraft. Changes in tangential acceleration can be achieved with a drag sail by following an on/off control law, where the 'on' and 'off' states correspond to orienting the sail perpendicular or parallel to the main force, respectively. Under this model, the area-to-mass ratio represents the 'control authority' for the sail, i.e. its capability to modify the nominal trajectory of the spacecraft, and it is used as the main parameter for the following sensitivity analysis.

Test cases are computed as follows. The maneuvering spacecraft is nominally assumed to be in de-orbiting phase, with the sail oriented perpendicular to the main force. Then, for each maneuver lead time the spacecraft with active sail is propagated backwards from the time of CA until the maneuver time. Finally, the sail is propagated forward without drag and SRP from the maneuver time to the nominal time of CA, and the new miss distance is evaluated. The CA and covariance information are taken from Conjunction Data Messages (CDMs) provided by ESA for a real CA at several warning times up to two days before the predicted CA*.

The results corresponding to a 2 days warning are given in Fig. 23. As expected, the miss distance in the nominal b-plane can be increased greatly with a long enough lead time, and it also shows a proportional increase with A/m. However, by taking a closer look at the results for small lead times it is observed that the miss distance in the b-plane initially decreases, reaching a minimum that moves towards higher separations and smaller lead times as the control authority A/m increases. Moreover, the collision probability also increases slightly for very short lead times, although it is possible to reach the 10^{-5} threshold for relatively short Δt. The justification for this behavior can be found in the b-plane. First of all, it is observed that displacement is mostly associated to time delay and not geometry change, as expected from a tangential thrust control. Furthermore, there is no periodic component unlike the maneuvering spacecraft case. By enhancing the area corresponding to short lead times, it is observed that the initial position in the b-plane lies at one side of the ellipse's principal direction, and the CAM makes the deviated position cross to the other side. Then, the maximum collision probability corresponds to the lead time for which the deviated position

*The actual data from the CDM, including the name of the spacecraft, cannot be reproduced here as it was provided under a NDA.

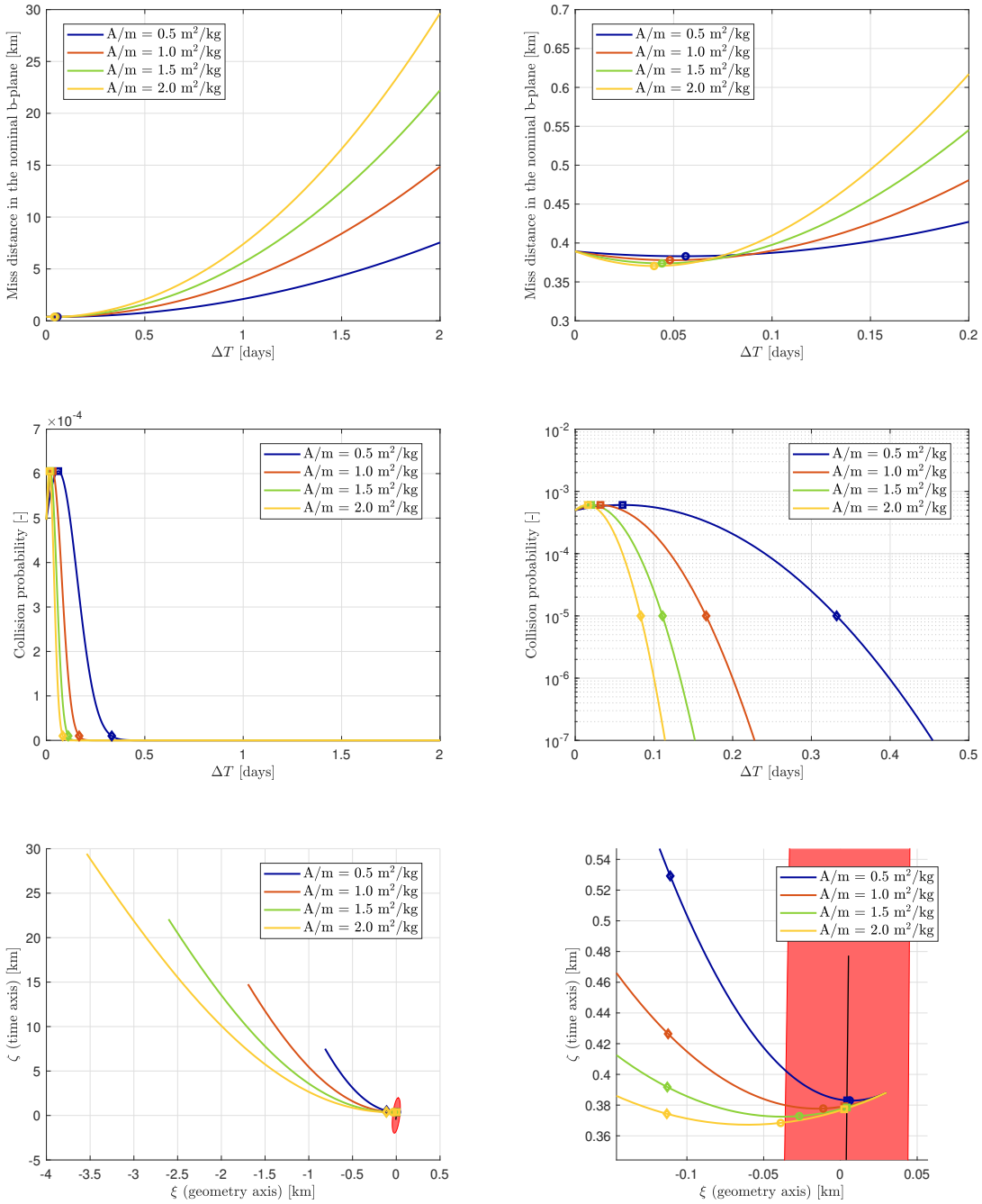

Figure 23. Miss distance, collision probability and b-plane representation for the 2 days warning CDM. Circles represent the minimum miss distance point, squares the maximum collision probability, and diamonds the crossing of the 10^{-5} collision probability threshold.

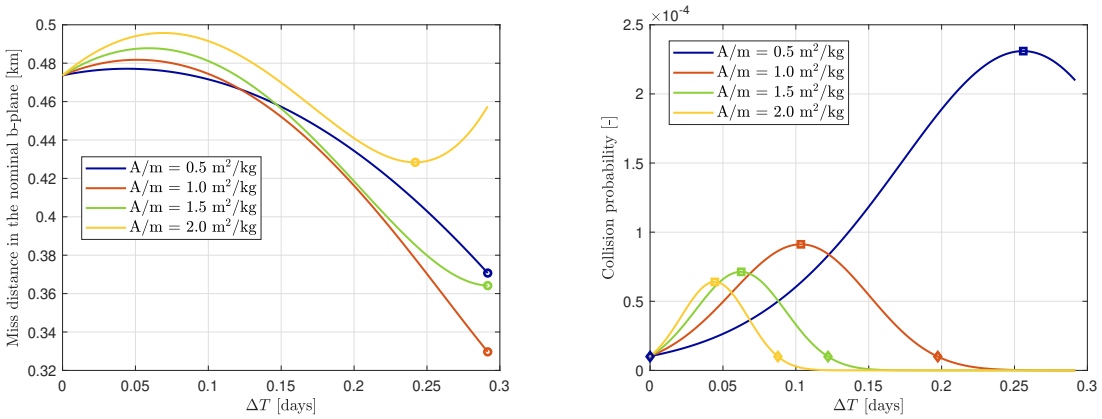

Figure 24. Miss distance and collision probability for the 7 hours warning CDM. Circles represent the minimum miss distance point, squares the maximum collision probability, and diamonds the crossing of the 10^{-5} collision probability threshold.

intersects this principal direction. On the other hand, the initial decrease in miss distance is related to the reduction in its ξ (as it crosses 0) and ζ components.

The initial increase in collision probability (and decrease in miss distance) may pose an additional difficulty for satellite operators deciding whether to perform a CAM or wait for a more updated CDM. Depending on the control authority of the sail, i.e. its area-to-mass ratio, and the geometry of the CA, there is a 'dead zone' or range of lead times for which it is not possible to effectively reduce the risk of collision. Any decision about a CAM has to be taken before this 'dead zone' is reached, limiting the operator's capability to wait for an updated, more accurate CDM to determine if the CAM is actually needed or not. The results for the CDM with 7 hours warning, Fig. 24, serve to illustrate this issue. All considered area-to-mass ratios fail to produce a substantial increase in miss distance, and actually reduce it for most lead times. Regarding collision probability, the sail with smaller A/m is not able to reduce it, as the corresponding 'dead zone' is longer than the available lead time. For this sail, the decision about performing or not the CAM would have to be taken with a previous CDM.

CONCLUSION

Collision avoidance maneuvers for passive de-orbiting missions involving sails have been studied in detail, considering different control strategies and taking into account the effect of uncertainties. An analytical model for the calculation of maximum deviation impulsive CAMs, both in terms of total separation and impact parameter in the b-plane, has been presented and its accuracy assessed. An extension of this model has also allowed to propagate the covariance matrices analytically for objects without a sail. When sails were involved, numerical orbit propagation using averaged dynamics has been used to account for the effect of drag and SRP.

As lead time for the CAM increases, both the covariance ellipse and the maximum δb CAM tend to align with the time axis in the b-plane, which limits the decrease in collision probability. Conversely, minimum collision probability CAMs tend to move along the geometrical axis for some configurations of the CA, resulting in a smaller miss distance. Analyzing the evolution of these CAMs in the b-plane has provided greater insight on the underlying dynamics. A key result is that the optimum $\delta \mathbf{v}$ for both CAM strategies tends to align with the transversal direction for lead times greater than half a period of the spacecraft's orbit.

Based on the previous result, a simple yet effective control law for the CAM of a de-orbiting sail has been proposed and studied, just by changing its orientation from normal to parallel to the main forces (drag and SRP). The numerical results show that the CAM is feasible for practical area-to-mass ratios and warning times, but an initial 'dead zone' in which it is not possible to reduce collision probability or miss distance

appears depending on the CA geometry on the b-plane. This introduces additional complexities for satellite operators, who have more time constraints when deciding whether to perform a CAM or wait for an updated CDM.

Numerical results show that drag and SRP do not introduce significant changes in the covariance for short lead times, typical of CAM maneuvers. Particularly, no significant variation in covariance size or orientation has been found for lead times up to 3 days.

Finally, the δv (impulsive) or A/m (sail) requirements have been reported for several CA configurations and lead times, showing the technological feasibility of this kind of CAMs for passive de-orbiting missions.

ACKNOWLEDGMENT

The research performed for this paper has received funding from the European Research Council (ERC) under the European Union's Horizon 2020 research and innovation programme within the project COMPASS (grant agreement No 679086). The simulations have been performed within the study contract "Environmental aspects of passive de-orbiting devices" funded by the European Space Agency (Space Debris Office) (contract number 4000119560/17/F/MOS).

REFERENCES

[1] C. Colombo, A. Rossi, F. Dalla Vedova, V. Braun, B. Bastida Virgili, and H. Krag, "Drag and Solar Sail Deorbiting: Re-Entry Time Versus Cumulative Collision Probability," *Proceedings of the 68th International Astronautical Congress*, Adelaide, Australia, 2017. IAC-17-A6.2.8.

[2] C. Colombo, A. Rossi, F. Dalla Vedova, A. Francesconi, C. Bombardelli, J. L. Gonzalo, P. Di Lizia, C. Giacomuzzo, S. Bayajid Khan, R. Garcia-Pelayo, V. Braun, B. Bastida Virgili, and H. Krag, "Environmental Aspects of Passive De-Orbiting Devices, Technical Note 1: Flux Analysis Using Passive De-Orbiting Systems, and Technical Note 2: Collision Consequences for Passive De-Orbit Devices," tech. rep., 2017.

[3] M. Vasile and C. Colombo, "Optimal impact strategies for asteroid deflection," *Journal of Guidance, Control, and Dynamics*, Vol. 31, No. 4, 2008, pp. 858–872. ISSN: 0731-5090 , doi: 10.2514/1.33432.

[4] C. Colombo, M. Vasile, and G. Radice, "Semi-analytical solution for the optimal low-thrust deflection of near-earth objects," *Journal of Guidance, Control, and Dynamics*, Vol. 32, No. 3, 2009, pp. 796–809. ISSN: 0731-5090 , doi: 10.2514/1.40363.

[5] B. A. Conway, "Near-optimal deflection of earth-approaching asteroids," *Journal of Guidance, Control, and Dynamics*, Vol. 24, No. 5, 2001, pp. 1035–1037. ISSN: 0731-5090 , doi: 10.2514/2.4814.

[6] S. Flegel, J. Gelhaus, C. Wiedemann, P. Vorsmann, M. Oswald, S. Stabroth, H. Klinkrad, and H. Krag, "The MASTER-2009 space debris environment model," *Fifth European Conference on Space Debris*, Vol. 672, 2009.

[7] T. T. Soong, *Fundamentals of probability and statistics for engineers*. John Wiley & Sons, 2004.

[8] R. Battin, *An Introduction to the Mathematics and Methods of Astrodynamics*. AIAA education series, American Institute of Aeronautics and Astronautics, 1999.

[9] J. L. Junkins and H. Schaub, *Analytical mechanics of space systems*. American Institute of Aeronautics and Astronautics, 2009.

[10] E. J. Opik, "Interplanetary encounters: close-range gravitational interactions," *Developments in Solar System and Space Science*, Vol. 2, Amsterdam, Elsevier Scientific Publishing Co, 1976.

[11] M. Petit, "Optimal Deflection Of Resonant Near-Earth Objects Using The B-Plane," Master's thesis, Politecnico di Milano, Department of Aerospace Science and Technology, July 2018. Advisor: Camilla Colombo.

[12] C. Bombardelli and J. Hernando-Ayuso, "Optimal impulsive collision avoidance in low earth orbit," *Journal of Guidance, Control, and Dynamics*, Vol. 38, No. 2, 2015, pp. 217–225.

[13] F. K. Chan, *Spacecraft collision probability*. Aerospace Press El Segundo, CA, 2008.

[14] F. K. Chan, "International space station collision probability," *The Aerospace Corporation, Chantilly, VA, USA*, 2009.

[15] C. Colombo, "Planetary Orbital Dynamics (PlanODyn) suite for long term propagation in perturbed environment," *6th International Conference on Astrodynamics Tools and Techniques (ICATT)*, Darmstadt, Germany, 14-17 March, 2016.